Analysis of in-situ measurements of Electron, Ion and Neutral Temperatures in the Lower Thermosphere-Ionosphere

Panagiotis Pirnaris[1] and Theodoros Sarris[1]

[1]Department of Electrical and Computer Engineering, Democritus University of Thrace, Xanthi, Greece

Correspondence: Panagiotis Pirnaris (ppyrnar@ee.duth.gr), Theodoros Sarris (tsarris@ee.duth.gr)

Abstract. Simultaneous knowledge of the temperatures of electrons, ions and neutrals is key to the understanding and quantification of energy transfer processes in planetary atmospheres. However, whereas electron and ion temperature measurements are routinely obtained from ground-based Incoherent Scatter Radars, simultaneous measurements of electron, ion and neutral temperature measurements can only be made in-situ. On the Earth's Lower Thermosphere-Ionosphere, the only available comprehensive in situ dataset of electron ion and neutral temperatures to date is that of the Atmosphere Explorers C, D and E, and the Dynamics Explorer 2 missions. In this study we first perform a cross-comparison of all co-temporal co-spatial measurements between in situ electron and ion temperature measurements from the above in situ spacecraft missions with corresponding measurements from the Arecibo, Millstone Hill, St. Santin Incoherent Scatter Radars, during times of overflights of these spacecraft over the radar fields of view. This expands upon a previous study that only considered data from the Atmosphere Explorer-C. The results indicate good agreement between satellite and ground-based radar measurements. Subsequently, out of the above datasets, all instances where ion temperatures appear to be lower than neutral temperatures are identified and are studied statistically. Whereas current understanding indicates that ion temperatures are generally expected to be higher than neutral temperatures in the Lower Thermosphere-Ionosphere, a non-negligible number of events is found where this does not hold true. The distribution of all such cases in altitude, latitude and longitude is presented and discussed. Potential causes leading to neutral temperatures being higher than ion temperatures are outlined, including both instrumental effects or measurement errors and physical causes. Whereas a conclusive case can not be made based on the present analysis, it is speculated from the results presented herein that not all cases can be attributed to instrument effects or measurement errors. This can have significant implications for the current understanding that the energy of the ions is expected to be higher than that of the neutrals, and points to the need for additional simultaneous in situ measurements in the LTI.

1 Introduction

It is well established that Earth's Lower Thermosphere-Ionosphere (LTI) region is generally not in thermal equilibrium, or, in other words, that $T_e > T_i > T_n$, where T_e, T_i and T_n represents the electron, ion and neutral temperatures respectively (see, e.g., Pfaff (2012)). The reason behind this expectation is that, whereas ions are heated by the electrons, they are cooled by conduction and collisions with the neutrals. The heat transferred to the ions is dependent on the electron temperature and the mean ion mass, or equivalently the H+ fraction and the plasma density. The cooling of ions is dependent on the neutral density.

The heat source could be influenced by the particle precipitation and frictional heating at high latitudes. The overall process of energy transfer between species, and the processes by which solar photon (in particular EUV) energy is stored as electron and ion energy, and is subsequently transferred to the neutrals, has been reviewed, e.g., by Richards (2022).

The quantification of all steps in the series of the complex processes affecting the energy transport between species is of critical importance to the state of the ionosphere, and addressing this topic requires simultaneous observations of all ionospheric parameters involved, over all local times, latitudes and altitudes of interest. In response to this need, in the early 1970's extensive measurements were performed in the Earth's thermosphere and ionosphere with the Atmosphere Explorer (AE) - C, -D, and -E satellites (see, e.g., Dalgarno et al. (1973)), which have provided simultaneous measurements of electron, ion and temperature measurements. Together with these measurements, ground-based Incoherent Scatter Radars (ISRs) routinely provide measurements of electron and ion temperatures; however, ISRs can not directly observe neutral temperatures. Thus, the above datasets of the AE-C, AE-D, AE-E and DE-2 missions are, to date, among the main sources for investigating the thermal equilibrium and energy transfer between electrons, ions and neutrals in the LTI. In particular, AE-C and AE-E have provided in situ measurements within the LTI at altitudes down to ∼130 km. These datasets constitute the basis of many empirical models of the ionosphere-thermosphere, such as the Naval Research Laboratory Mass Spectrometer and Incoherent Scatter Radar (NRLMSIS) (e.g., Picone et al. (2002), Emmert et al. (2021)) and the International Reference Ionosphere (IRI) (e.g., Bilitza et al. (1993), Bilitza et al. (2022)), and led to a leap in our knowledge in thermospheric research, as summarized in, e.g., Schunk and Nagy (2009). Measurements from the Atmosphere Explorers were complemented by the Dynamics Explorers 1 and 2 in the early 1980's (see, e.g., Burch and Hoffman (1985)), which reached altitudes down to ∼ 250 km, and which also included instrumentation that provided simultaneous measurements of electron, ion and neutral temperature. Later on, observations of T_n in the lower thermosphere have also been provided from space-born UV instruments, such as GUVI on the TIMED satellite, whereas (Peterson et al., 2023) analyzed these measurements and showed that co-temporal, co-spatial observations of electron, ion and neutral temperatures are possible when this dataset is combined with measurements from incoherent scatter radars.

Despite significant progress in the understanding of key LTI processes since the times of the early AEs and DEs, there are many aspects of the processes taking place in the LTI region that are still not well understood; open topics have been highlighted by, e.g., Sarris (2019), Palmroth et al. (2021), Sarris et al. (2020), and Peterson (2021). In particular, Peterson (2021) highlighted the lack of a quantitative understanding of the state of thermal equilibrium of the LTI, which reflects the complexity of the physics of the LTI region, and which arises due to the lack of a large and systematic data base of simultaneous neutral, ion, and electron densities and temperatures. Based on rocket measurements, Sasaki and Kawashima (1975b) have shown altitude profiles of electron, ion and neutral temperatures, with distinct occurrences of $T_i < T_n$ being observed at or below 120 km as well as between 130 km and 140 km. Recently, analyzing electron, ion and neutral temperature profiles from simultaneous observations for case studies from AE–C when it was located at altitudes below ∼ 140 km together with quiet-time neutral observations over Millstone Hill radar, Peterson et al. (2023) re-addressed the current status and presented key challenges and open issues of research, based on events where the above-stated condition that $T_e > T_i > T_n$ does not hold true. They concluded that instrumental uncertainties or the spatial/temporal aliasing are a possible explanation, but they also

60   left open the potential of uncertainties in our quantification and understanding of processes in the LTI, highlighting the need for new measurements.

     In this study, we revisit this issue of the relative temperatures between species by harvesting existing datasets of co-temporal, co-spatial measurements. We first perform an inter-comparison of in situ measurements of electron and ion temperatures from the AE-C, AE-D, AE-E and DE-2 measurements with the corresponding measurements from ISRs, during times of over-flights

65   of these missions over the fields of views of the radars, in order to illuminate possibilities of observational uncertainties in the in-situ measurements, such as potential systematic errors in the in-situ electron and ion temperature measurements. A similar correlation analysis has been performed for a limited subset of the above measurements by Benson et al. (1977a), who compared the in-situ measurements of T_e and T_i, delivered by AE-C, during overpasses from the fields of view of Incoherent Scatter Radar, concluding that AE-C is in good agreement with ISRs. To this direction, further to the comparisons of measurements

70   by AE-C during over-flights in the fields of view of Arecibo, Milestone Hill, Jicamarca and Saint Santin Incoherent Scatter Radars (ISRs) that were performed by Benson et al. (1977a), we investigate in addition measurements from AE-D and -E, as well as from DE-2 during flights over the same radars, following the same analysis procedures as in Benson et al. (1977a). Subsequently, we identify cases where $T_i < T_n$ and we investigate the appearance of such events statistically by plotting their distribution in altitude as well as in latitude vs. longitude.

75   This paper is organized as follows: Section 2 presents the datasets from the satellites and ISRs that are used in this work. Section 3 presents the statistical distributions that result from the analysis of these datasets, focusing on the appearance of cases where $T_i < T_n$. Section 4 discusses the results, emphasizing the possible factors contributing to observed distributions of the cases where $T_i < T_n$. Finally, the concluding remarks in Section 5 encapsulate the outcomes derived from the data analyzed in this study and point to future measurements needed in order to resolve this key open science issue that is related to the energy

80   transfer and thermal equilibrium in the LTI.

2   Datasets

2.1   In situ Electron, Ion and Neutral Temperature Measurements

With the exception of one rocket observation (Sasaki and Kawashima, 1975a), the only in-situ co-temporal, co-spatial observations of T_e, T_i and T_n within the LTI were obtained from satellites AE-C, AE-D and AE-E in the 1970's and early 1980's.

85   T_e measurements on board all three AE satellites have been obtained via the Cylindrical Electrostatic Probe (CEP) instruments (Brace et al. (1973); Benson et al. (1977b)), which are retarding potential Langmuir probe devices, providing electron temperature measurements by the current-voltage (I-V) characteristic relationship of the Debye sheath (Schwabedissen et al. (1997); Hopwood et al. (1993); Stanojević et al. (1999); Chen and Sekiguchi (1965); Block (1978)). T_i measurements have been obtained from the Retarding Potential Analyzer (RPA) onboard the AE satellites (Hanson et al. (1973); Hanson and Heelis

90   (1975)) and onboard the DE-2 satellite (Hanson et al. (1981)), which provide ion temperature by I-V characteristics delivered by the instruments (Hanson et al. (1973); Nenovski et al. (1980); Hanson et al. (1972); Whipple (1961)). Similar RPAs have also been used in other space missions, such as the LAICE and DMSP satellites. Finally, T_n measurements have been obtained

through the Neutral Atmosphere Temperature (NATE) instrument onboard the AE satellites (Spencer et al. (1973a, 1974, 1976); Chandra et al. (1976)), and through the Neutral Mass Spectrometer (NMS) (Carignan et al. (1981)) onboard the DE-2 satellite.

95 NATE and NMS provide neutral temperature through the determination of the velocity distribution of the molecules (Spencer et al. (1973a); Carignan et al. (1981)).

In this study, we focus on the comparison between T_i and T_n measurements; however, T_e measurements are also considered as part of the cross-comparison with ISR T_e and T_i data, for completeness of the comparison through the extension of the work of Benson et al. (1977a) to all available in situ satellite databases.

100 ## 2.2   Remote Sensing Electron and Ion Temperature Measurements

As a first step of the comparative analysis between in-situ and remote sensing measurements of T_e and T_i, all conjunctions between the in-situ datasets and ISRs measurements were identified. Remote sensing measurements were obtained through a collection of different ISR experiments, which are maintained at the Madrigal Database, an upper atmospheric science database used by scientific groups around the world. Madrigal was created and launched at MIT Haystack in the 1980s, prior to being
105 adopted as the basis for the Coupling, Energetics and Dynamics of Atmospheric Regions (CEDAR) program database. The names, geographic coordinates and L-shells of the ISR facilities used in this study are as follows: Arecibo (18.4^oN, 66.8^oW, $L = 1.4$), St. Santin (44.6^oN, 2.2^oE, $L = 1.8$) and Millstone Hill (42.6^oN, 71.5^oW, $L = 3.1$). The L-shell here represents the McIlwain L, a parameter describing the magnetic field lines which cross the Earth's magnetic equator at a number of Earth-radii equal to the L-value. The criteria in order to mark a satellite over-pass over a radar field of view as a conjunction
110 are as follows: Latitude Range: $\pm$ 0.5 degree, Longitude Range: $\pm$ 18 degrees, Altitude Range: $\pm$ 10 km, Time Range: $\pm$ 60 minutes. These conjunction criteria are identical to the ones used in Benson et al. (1977a), so as to be able to cross-compare the extended datasets that are presented herein with their results. The common dataset for each satellite and ISR is available on (Pirnaris and Sarris (2023)).

The total number of conjunctions with valid T_e measurements between each of the satellites and all the above ISRs is as
115 follows: AE-C: 79, AE-D: 0, AE-E: 0, DE-2: 65, leading to a total of 144 measurements. The total number of conjunctions with valid T_i measurements between each of the satellites and all the above ISRs is as follows: AE-C: 63, AE-D: 3, AE-E: 46, DE-2: 47, leading to a total of 159 conjunctions. In comparison, the study of Benson et al. (1977a) was based on a total of 39 conjunctions for T_e and 27 conjunctions for T_i.

2.3   Comparison of Satellite and Incoherent Scatter T_e and T_i measurements

120 Figure 1 presents the results of the comparison between T_e (left) and T_i (right), for the conjunctions between the in-situ and ISR measurements as listed above. In this figure, conjunctions of AE-C with all three ISRs (i.e., Arecibo, Millstone Hill and St. Santin) are marked in blue; conjunctions of AE-E with ISRs are marked in green; and conjunctions of DE-2 with ISRs are marked in red. Linear fits trough these data points are shown in blue, green and red lines, corresponding to the above datasets; the equations of the linear fits are shown along the colored lines. In addition, the ratio between the satellite (SAT) and radar
125 (ISR) measurements has been calculated according to $R_{T_k} = T_{k(SAT)}/T_{k(ISR)}$, where $k = e$ for electrons and i for ions. The
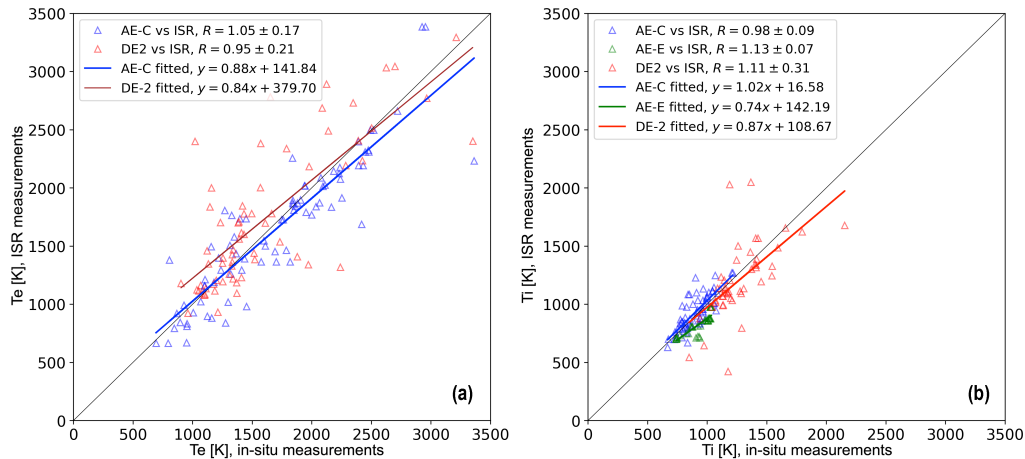
Figure 1. (a) Correlation between in situ measurements of T_e from AE-C (blue) and DE-2 (red) and corresponding ISR measurements, during times of conjunctions. (b) Correlation between T_i measurements between in situ measurements of of AE-C (blue), AE-E (green) and DE-2 (red), during times of conjunctions with ISRs. Lines in both plots shows linear fits. The linear fit parameters are marked in the insets of both plots

numerical values of these ratios are shown in the legend in the upper left corner of each figure. It is noted that AE-D included only 3 T_i measurement conjunctions, and a similar fit is not presented in the above analysis.

The results shown in Fig. 1(a) and 1(b) indicate that AE-C and ISR data yield similar measurements for both T_e and T_i during their conjunctions. This is consistent with the findings of the study by Benson et al. (1977a). Following the same approach and extending the work of Benson et al. (1977a), Fig. 1a also presents T_e measurements from DE-2 and ISRs during times of conjunctions. The comparisons show that DE-2 measurements have a slope that is lower than 1, meaning that DE-2 systematically measures higher electron temperatures than the ISRs. It is noted that no conjugated measurements of T_e were found between AE-E and ISRs. Similarly, Fig. 1bpresents T_i measurements from AE-E and DE-2 during times of their conjunctions with ISRs; the comparisons between both AE-E and DE-2 with ISRs during times of their conjunctions yield slopes that are lower than 1, meaning that both AE-E and DE-2 systematically report higher ion temperatures than the ISRs. This could indicate the need for systematic re-calibration of AE-E and DE-2 measurements, whereby AE-E and DE-2 measurements might need to be systematically lowered.

In addition to the correlation between in situ and ISR measurements of T_e and T_i that is shown in Fig. 1, the comparative analysis was extended by estimating also the ratio between in-situ and ISR measurements as a function of local time, absolute longitude and altitude; these results are included as supplementary material Fig. A1 and A2 for T_e and T_i comparisons, respectively. Figures A1 and A2 are plotted in the same format as in Fig. 2 of Benson et al. (1977a), to allow for cross-comparisons with that study. The numbers in the lower right corner in each panel of Fig. A1 and A2 indicate the ratio between satellite and radar measurements. From Fig. A1 and A2 it it can be seen that the conjunctions are well distributed over local time, absolute longitude separation between the satellites and radars, and altitude. Furthermore, in Fig. A1 and A2 we also plot the number

of measurements as a function of the in situ (SAT) over radar (ISR) measurements, in order to visualize the distribution of the measurements under comparison over local time, absolute longitude separation and altitude. The estimated linear fits in these figures are in agreement with the results from Benson et al. (1977a), in particular for T_e for all satellites and T_i for AE-C and AE-D. However, a larger standard deviation is observed in the linear fit of T_i measurements from DE-2 with respect to the ISR measurements. This is more evident for high T_i, with satellite measurements appearing to underestimate T_i compared to ISRs. Finally, in Fig. A3 we plot histograms of measurements distribution over the calculated ratio. Figure A3 is plotted in the same format as in Fig. 3 of Benson et al. (1977a), allowing for comparisons between the two studies.

3 Comparisons between in-situ Ion and Neutral Temperatures

This section presents an analysis of the comparison between T_i and T_n as measured simultaneously onboard satellites AE-C, AE-D, AE-E and DE-2, focusing in particular on the distribution in altitude, latitude and longitude of cases where $T_i < T_n$. The purpose of this analysis is to comment on the causes (either instrumental or physical) behind deviations from the commonly held perception that T_i is generally expected to be greater than T_n in the LTI.

3.1 Dataset

As a first step, from the entire database of T_i and T_n measurements obtained from satellites AE-C, AE-D, AE-E and DE-2, data were only considered when the satellites were located below 500 km. From this subset, all cases with simultaneously valid T_i and T_n measurements were selected. For the selection of valid data points, the WATS instrument data processing of DE-2 was followed (NASA (1998)). As part of this process, temperatures in the datasets were considered as valid when the condition $200 \leq T_k \leq 4000$ was met, where $k = e, i, n$. After subtracting all data points flagged as erroneous, the dataset of temperature measurements where T_i and T_n are simultaneously valid consists of 52,822, 11,960, 171,775 and 236,785 data points for satellites AE-C, AE-D, AE-E and DE-2, respectively.

Subsequently, the subset of measurements when $T_i < T_n$ was identified for each satellite. From this subset, only data points where $T_i < T_n$ appeared at consecutive points along the orbit were considered, whereas individual (i.e., non-sequential, or singleton) points were discarded. Within this dataset from satellites AE-C, AE-D, AE-E and DE-2, the condition that $T_i < T_n$ was met in 18,959, 2,934, 4,501 and 10,674 data points respectively, corresponding to 36 %, 25 %, 3 % and 5 % of the total numbers of valid data points respectively. These numbers indicate that there is a non-negligible occurrence rate of cases when neutrals are (or appear to be) hotter that ions.

In the following we first present two examples of such events where the condition $T_i < T_n$ is observed; we then proceed to investigate the statistical distributions of these events, both in altitude and in longitude vs. latitude.

3.2 Test cases of $T_i < T_n$ events

An example of such event occurred on January 17, 1975, during orbit 5089 of AE-C. An overview is shown in Fig. 2, where in the first three panels the spacecraft altitude, latitude and L-shell are plotted, whereas in the fourth panel T_i and T_n are plotted
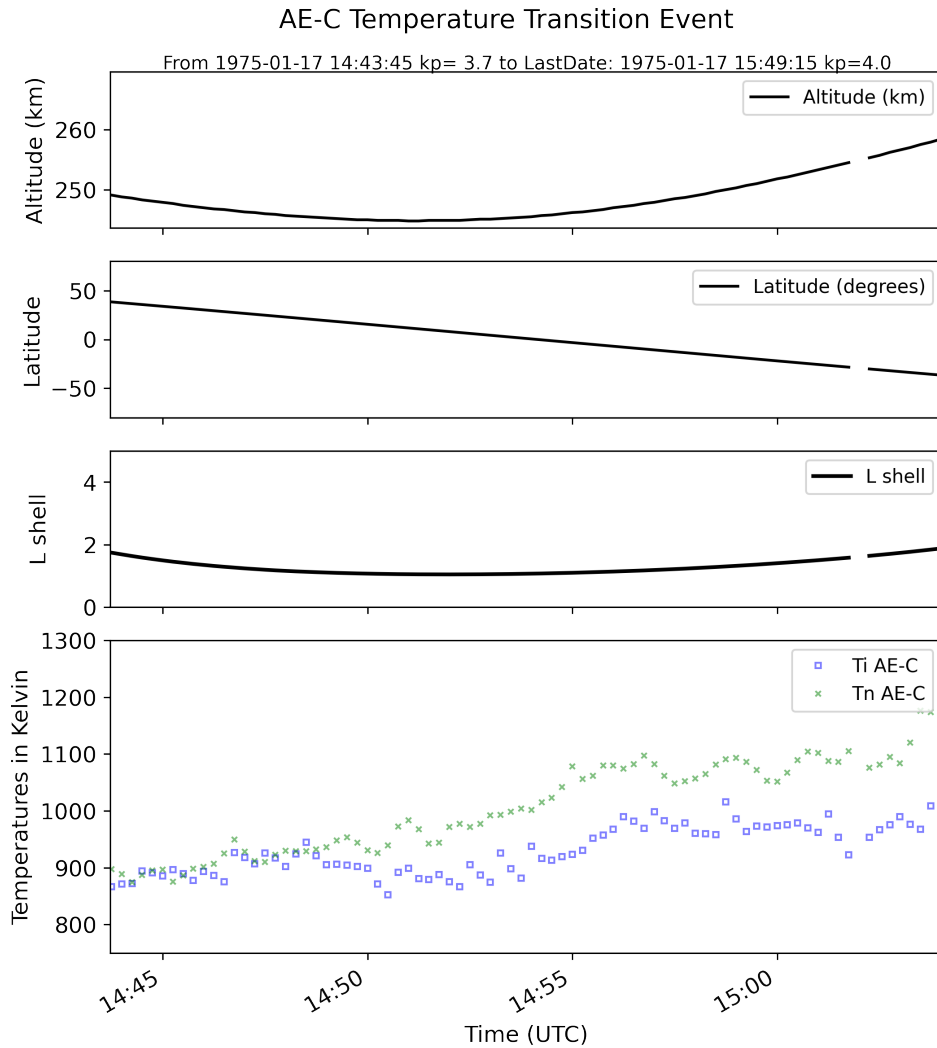
Figure 2. (a) Altitude, (b) Geographic latitude, (c) L-shell and (d) T_i (blue) and T_n (green), for AE-C orbit No 5089, on January 17, 1975, 14:43 to 15:49 UT.

in blue and green, respectively. Solar and geomagnetic indices during the time of this event were as follows: Dst ranged from -17 nT to -15 nT, AE ranged from -172 to -62, and kp ranged from 3+ to 4, indicating moderate geomagnetic activity levels.

The second example, plotted in Fig. 3, shows a sequence of 5 DE-2 orbits. During this event, the transition from $T_i \geq T_n$ (first orbit) to $T_i < T_n$ (second to fifth orbits) is observed. Solar and geomagnetic indices during this time are as follows: $Dst = -44$, $AE = 81$ and $Kp = 2-$ to 4, indicating low to moderate geomagnetic activity levels. It is noted that between each orbit there are data gaps in the DE-2 dataset.

The ground tracks of these events are shown in Fig. 5, where the ground track of the AE-C orbit of Fig. 2 is shown with a solid line, whereas the ground tracks of the 5 consecutive DE-2 orbits of Fig. 3 are shown with 5 dashed lines.
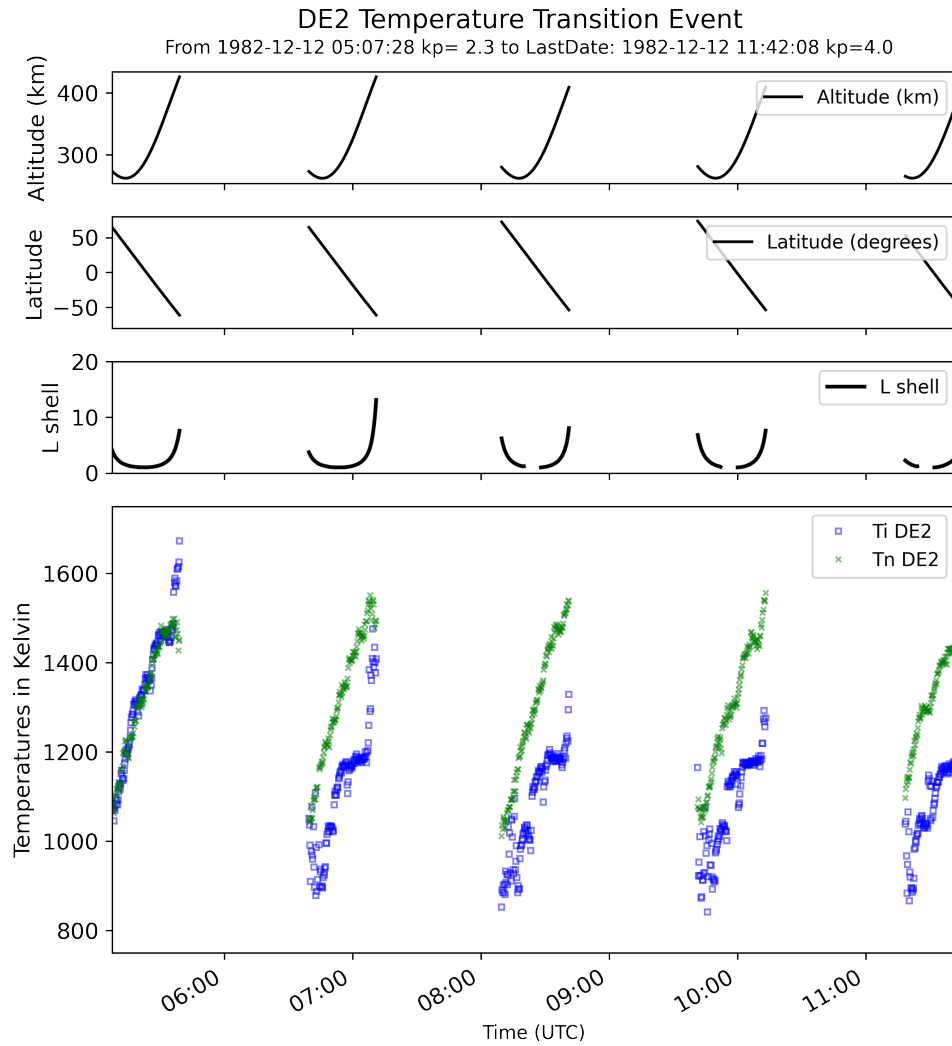
Figure 3. a) Altitude, (b) Geographic latitude, (c) L-shell and (d) T_i (blue) and T_n (green), for DE-2 orbits 7491 to 7495, on December 12, 1982, 05:07 to 11:42 UT.
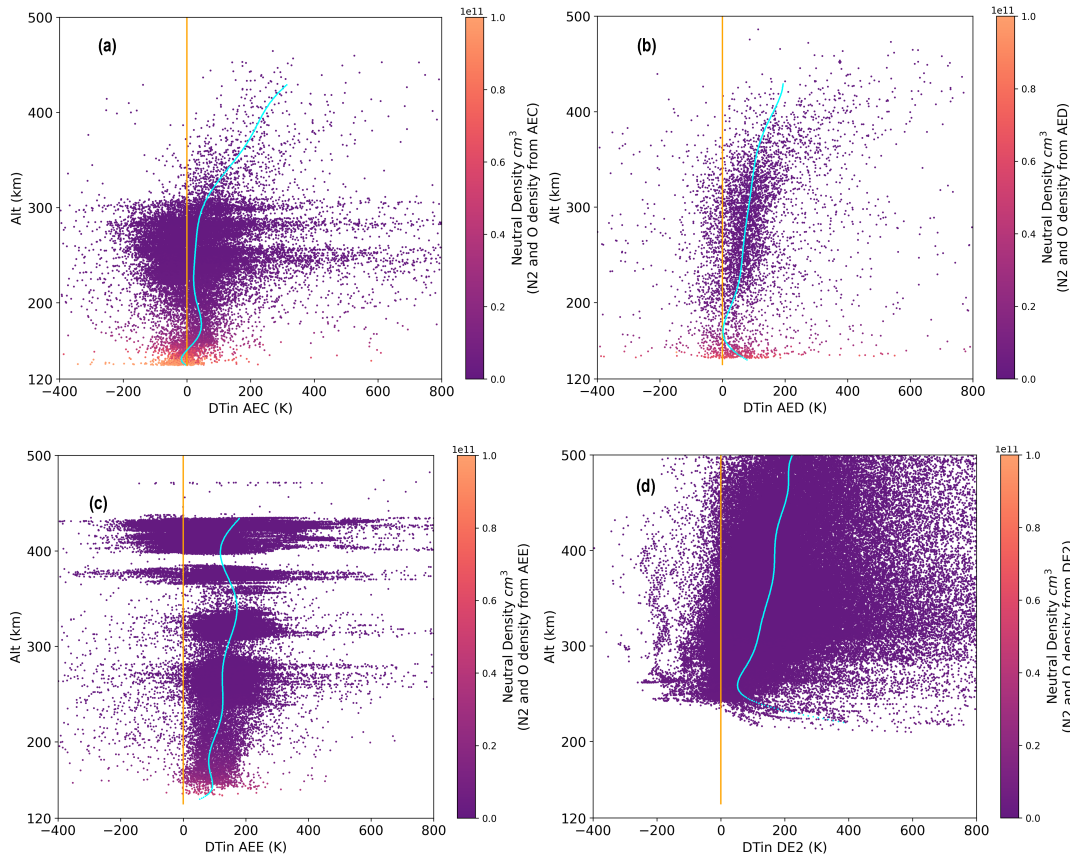
Figure 4. ΔT_{in} for the various satellite datasets, as marked. (a) ΔT_{in} vs Alt (km) for AE-C, (b) ΔT_{in} vs Alt (km) for AE-D, (c) ΔT_{in} vs Alt (km) for AE-E and (d) ΔT_{in} vs Alt (km) for DE-2. The color scale of the data points represents the neutral density, as obtained from the addition of N_2 and O in-situ density measurements.

3.3 Spatial Distribution of $T_i < T_n$ cases

185 In Fig. 4 we plot all the occurrences of $\Delta T_{in} = T_i - T_n$ (both positive and negative) as a function of altitude, separately for each spacecraft. To this direction, panels (a) through (d) of Fig. 4 present the altitude distribution of all ΔT_{in} for AE-C, AE-D, AE-E and DE-2, respectively. The temperature of thermal equilibrium between ions and neutrals, or $\Delta T_{in} = 0$, is plotted with an orange line, whereas the local mean of ΔT_{in} is plotted with a light blue line; the local mean was calculated at altitude steps of 5 km. As it can be seen in these panels, whereas the local mean shows a positive average ΔT_{in} for all missions at all altitudes

190 (with the exception of the lowermost altitudes of AE-C), there is a non-negligible number of cases where negative differences are observed. Furthermore, these plots show a positive trend of ΔT_{in} with altitude, meaning that cases of $\Delta T_{in} < 0$ are more likely to be observed at lower altitudes.
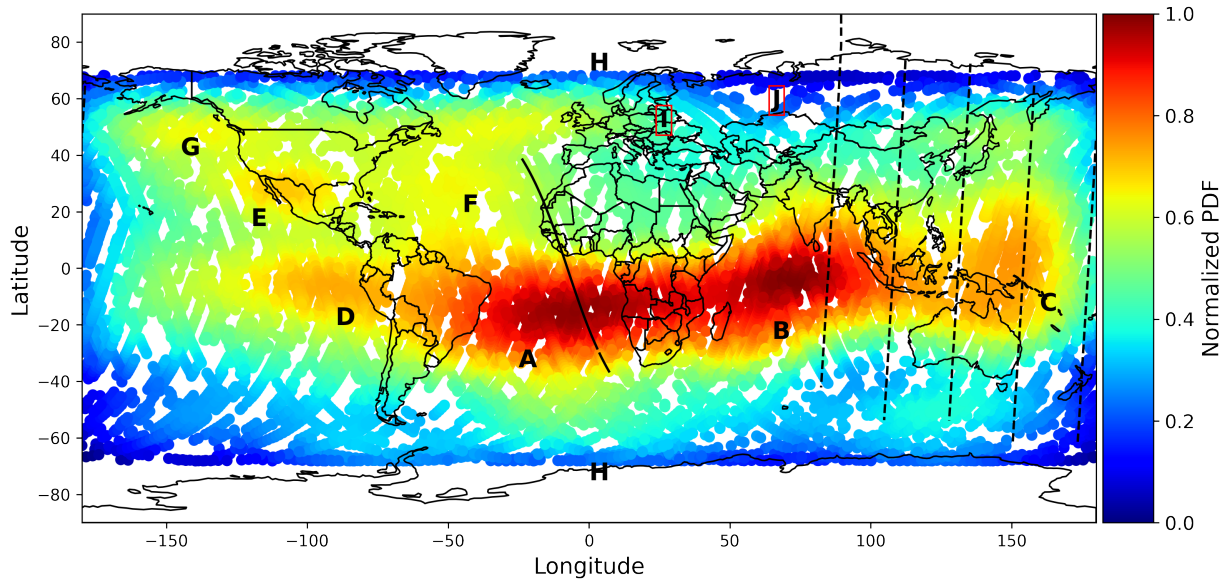
Figure 5. Probability of occurrence of $\Delta T_{in} < 0$ in AE-C measurements of T_i and T_n. The solid black line represents orbit No. 5089 of AE-C (Fig. 2), whereas dashed black lines represent orbits No. 7491 to 7495 of DE-2 shown in Fig. 3. The color scale represents the normalized Probability Distribution Function, ranging from 0 (corresponding to the lowest likelihood for the observation of $T_i < T_n$), which is marked as blue, to 1 (corresponding to the highest likelihood), which is marked as red.

In Fig. 5 we plot the distribution of all cases where $T_i < T_n$ (such as those shown in Fig. 2 and 3) as a function of geographic latitude and longitude. The geographic distribution of the $T_i < T_n$ cases is depicted by plotting the corresponding Probability Distribution Function (PDF) (Billingsley (1986)) of the occurrence of such events. The PDF is calculated based on the Kernel Density Estimation (KDE) method (e.g., Rossini (2000); Rosenblatt (1956), Scott (1992)), using Gaussian kernels. More specifically, as part of the fundamental principle of a Gaussian KDE, each data point is given a Gaussian distribution (kernel), and these distributions are subsequently added up to produce a smooth approximation of the underlying probability density. The results are then normalized to produce the relative (unit-less) likelihood. The normalization is performed by subtracting the lowest value that is observed on the map from the PDF value at each point and subsequently dividing by the range from maximum to minimum PDF value; thus the resulting values range from 0 (corresponding to the lowest likelihood for the observation of $T_i < T_n$), which is marked as blue in 5, to 1 (corresponding to the highest likelihood), which is marked as red. In 5, the solid line marks the orbit of AE-C on January 17, 1975 that corresponds to the sample event shown in Fig. 2, and the 5 dashed lines mark the orbits of DE-2 on December 12, 1982 that correspond to the event shown in Fig. 3. Letters A through J indicate regions of interest that are discussed in further detail in the section below.

4   Discussion

In the following, we discuss possible reasons leading to the appearance and distribution of the occurrences of $\Delta T_{in} < 0$. Both potential instrumental or measurement effects and physical processes are discussed, including implications for our current understanding of LTI processes.

4.1   Possible sources of measurement errors

There are several potential sources of uncertainty that can lead to systematic and random errors in the in-situ measurement of temperatures in space. The removal or correction of such errors has been the topic of multiple studies over the past decades (e.g., DeForest (1972), Whipple (1981), Hastings (1995), Ergun et al. (2021), Hanley et al. (2021)). These errors are primarily due to the high spacecraft velocity and the interaction of the spacecraft with the surrounding plasma and neutral environment. For example, factors that affect the accuracy of measuring ion temperatures include the acceleration of plasma by a charged surface, the generation of a complex plasma cloud that surrounds the spacecraft and interacts with the environment, and impact ionization and reflection of particles off of the spacecraft and the subsequent inclusion of reflected ions in the measurements (e.g.,Heelis and Hanson (1998); Ergun et al. (2021); Hanley et al. (2021)). In particular, Ergun et al. (2021) addressed space-craft motion effects due to the creation of a wake in the Martian ionosphere, and demonstrated the recalibration of MAVEN instrumentation on the Mars Atmosphere and Volatile EvolutionN (MAVEN) spacecraft (Jakosky et al. (2015)) with the aid of kinetic solutions and published results from laboratory experiments, through which they achieved a significant improvement in the systematic uncertainty of T_e measurements. Similarly, Hanley et al. (2021) discussed a series of rigorous processes that they employed to identify and correct various sources of uncertainties in measurements of T_i arising from the supersonic velocities of MAVEN; these include altitude-dependent systematic errors as well as random errors from statistical fluctuations and uncertainties in spacecraft potential.

Based on the general agreement between in-situ and ISR estimations of T_i, it is noted that T_i measurements are less likely than T_n to include large systematic deviations that could lead to the appearance of $\Delta T_{in} < 0$ in a statistically significant percentage of the total number of measurements, indicating that these measurements are less likely to be considered as outliers. Factors affecting the accuracy of neutral temperature measurements include the applicability of the kinetic theory used in extracting neutral temperatures, in particular at lower altitudes where a shorter mean-free-path of the measured particles might affect the measurements, and gas-surface interactions, which are also dependent on altitude and neutral density (e.g., Spencer et al. (1973b)).

The altitude dependence that is shown by the light blue curves of Fig. 4 indicates that the appearance of $\Delta T_{in} < 0$ could be dependent on such spacecraft-environment interaction effects, which are expected to be dependent on neutral density. This effect could account for the larger appearance of $\Delta T_{in} < 0$ at altitudes below 150 km, as is shown, for example, in AE-C measurements; however, as it can be seen in Fig. 4(a), in the altitude ranges from ∼150 km to 200 km there is a decrease in the appearance of such events, which are again enhanced at altitudes upwards of 200 km.

4.2 Possible physical mechanisms that could lead to observations of $T_i < T_n$

The structured appearance of the occurrence rates of the $\Delta T_{in} < 0$ events in Fig. 5 (as opposed to an even or random distribution of such events in latitude and longitude) indicates that there are, potentially, distinct underlying mechanisms leading to either the enhancement of neutral temperatures or the decrease of ion temperatures in these regions. In the following, the regions of enhanced probability for the appearance of $\Delta T_{in} < 0$ events are discussed, followed by a discussion on possible physical underlying mechanisms that could be the cause of these observations. It is noted that the analysis presented herein is only meant to highlight these intriguing results, and to point to potential mechanisms, but can not, at this point, yield a dominant mechanism or combination of mechanisms that can conclusively explain these results.

In Fig. 5, there seven distinct regions of enhanced occurrences of $\Delta T_{in} < 0$ measurements; these are marked from A through G, as follows: There are four primary peaks of high occurrences, marked as A through D, that are located close to the geomagnetic equator. Out of these, A and B are located in the South Atlantic and Indian Oceans, respectively, whereas secondary peaks marked as C and D are observed in the Western and Eastern Pacific Ocean, respectively. A distinct enhancement is observed in the North Mexico/Baja California region, and is marked as E. An enhancement is also observed in the Northern Atlantic Ocean (as compared, e.g., to the continental regions of Northern America and Europe), and is marked as F. A distinct peak can be observed off-of the southern coast of Alaska and Western Canada (compared to the corresponding continental regions), and is marked as G. Furthermore, there are four regions which have distinctly smaller concentrations of observations of $\Delta T_{in} < 0$ events: these are observed in the Northern and Southern high latitude regions, which are marked as H; in the European continental region, which is marked as I; and in the Northern Russia region, which is marked as J.

A first candidate mechanism that can significantly impact the LTI, altering neutral temperatures, concerns Gravity Waves (GW). Gravity waves are dissipated in the thermosphere at altitudes between 100 and 200 km through molecular damping, modifying thermospheric temperatures (Walterscheid (1981)). Gravity waves generally form in the troposphere and lead to the transfer of momentum from the troposphere to the stratosphere and mesosphere, and even further upwards to the thermosphere (Fritts and Alexander (2003)). These waves propagate upwards from the troposphere, and, in doing so, they grow exponentially in terms of wave amplitude (e.g. Andrews et al. (1987)). The subsequent wave breaking of these large-amplitude waves leads to significant energy and momentum deposition. The detailed parameterization of GWs is an open issue in upper atmosphere research, in particular for medium (meso-β) and small scale (or meso- γ) GWs, measurements of which are completely lacking (see e.g., Liu (2019)), and whose effects could be significant for LTI energetics and dynamics.

The heating and cooling effects of GWs in the thermosphere have been extensively investigated by many simulation studies. For example, Yiğit and Medvedev (2009) used a GW parameterization that was specifically designed for thermospheric heights, which was implemented in the Coupled Middle Atmosphere & Thermosphere model (CMAT2) Global Circulation Model (Harris (2001) and Dobbin (2005)), covering altitudes from the tropopause to the F2 region. They performed simulations for the June solstice, and illustrated the regions of GW heating and cooling rates. The simulation results indicated significant irreversible heating in the high latitudes of both hemispheres, which reached 90 to 100 K per day near 200–210 km; secondary peaks in heating also appeared in the tropics, predominately below 130–140 km, which reached up to 10 K per day. Such

preferential heating of the neutrals by GWs is compatible with the observations presented herein. However, even though regionally GWs can lead to significant heating in the thermosphere, Yiğit and Medvedev (2009) note that, the net thermal effects of GWs is primarily cooling of the thermosphere, and that the simulated model temperatures can be decreased by up to 200K at the summer pole and by 100 to 170K at other latitudes near 210 km. Simulations by England et al. (2020) also show that GWs can lead to cooling of the neutrals in the LTI at altitudes above 210 km.

GWs can be generated through a range of different processes: these can be of meteorological origin (convective, shear, geostrophic), topographic origin (e.g., mountain waves) or even due to strong tropospheric disturbances. In the following we discuss the generation mechanisms and localizations in relation to the appearance of $\Delta T_{in} < 0$ events.

Intense GWs are known to be generated by winds flowing over mountain formations; for example, Hierro et al. (2018) reported the appearance of GWs over the Andes. However, whereas peak D could possibly be associated with the Andes, there no corresponding signals over North America (Rocky Mountains), Europe (Alps), or India/China (Himalayas); this indicates that there is possibly no clear association of $\Delta T_{in} < 0$ events with GWs of topographic origin.

Together with mountain ranges, GWs are known to be generated by hurricanes, typhoons and tropical cyclones. In order to find potential correlations with such dynamical tropospheric events, all relevant occurrences of hurricanes, typhoons and tropical cyclones combined were collected from the NOAA IBTrACS v4 (Knapp et al. (2010) and Knapp et al. (2018)) database, and are plotted in Fig. A4 for the time period from 1974 to 1976 corresponding to the period of in situ measurements that are plotted in Fig. 5. It is noted that the region marked as E and F in Fig. 5, and in particular the region extending from $\sim 18^o$ to $\sim 40^o$ latitude and $\sim -120^o$ to $\sim -80^o$, has a particularly high occurrence rate of Hurricanes and Typhoons and a markedly similar extent in their localizations. The same is observed in the region of the Indian Ocean and north of Australia, from $\sim 10^o$ to $\sim -40^o$ latitude and $\sim 40^o$ to $\sim -150^o$, which has a particularly high occurrence rate of tropical cyclones. However, no such events are observed over the regions marked as A, B and D, meaning that different mechanisms are taking place in these regions.

Together with the above regions of dynamical tropospheric events, such as hurricanes, typhoons and cyclones, and the appearance of GWs in association with large mountain formations, there are many other triggers of highly localized and persistent GWs: for example, such phenomenology has been termed a "GW hot spot", appearing over specific regions and times (e.g., Becker et al. (2022)). Other studies have reported the lack of GWs over specific regions: for example, resulting from the diurnal tide's strong poleward winds over the European area, some GWs were found to be moving westward across the Atlantic and eastward over eastern Europe (e.g., Becker et al. (2022)), leaving a gap in terms of GW occurrence over Europe. Investigating in detail the appearances of these localizations and their causes is a topic that is beyond the scope of this paper, and that is left for future studies.

Recently, Vadas and Azeem (2021) reported on GWs that can cause up to 75° K changes at 200 km. Interestingly, they report that the locations of these GWs, even though orographically generated, they are not centered on mountains, but instead radiate from them. They also reported that these GWs are attenuated by horizontal magnetic fields, and that they could be located 1 or 2 days after a large polar vortex event. These results indicate that the correlation between the generation mechanism, the region and the effects of GWs can be a much more complicated process than currently thought.

Another potential mechanism that could lead to an enhancement of T_n and hence to the appearance of instances of $\Delta T_{in} < 0$ could be associated with the equatorial region fountain effect: during this process, the plasma is driven upwards due to an $\boldsymbol{E}x\boldsymbol{B}$ drift, owing to the eastward direction of $\boldsymbol{E}$ and the northward (parallel to the Earth's surface) direction of $\boldsymbol{B}$. The plasma motion drives the neutral gas to move upwards as well, through the momentum transferred via collisions between neutral and charged particles, transferring momentum from the plasma to the neutral gas. These collisions end up heating the neutral gas, whose temperature is gradually enhanced. At higher altitudes, the $\boldsymbol{E}x\boldsymbol{B}$ drift stops driving the plasma upwards, which, in the absence of an electric field, follows the magnetic field lines, mapping to latitudes northwards and southwards of the magnetic equator. This process leaves the heated neutrals with an average temperature T_n that is higher than the ion temperature T_i.

An additional candidate mechanism that could lead to the appearance of $\Delta T_{in} < 0$ is related to the South Atlantic Anomaly (SAA), the region over the South Atlantic Ocean where the magnetic field strength is significantly weaker than in other parts of the planet (Yoshida et al. (1960),Vernov and Chudakov (1960) and Ginzburg et al. (1962)): the low altitude of the mirroring point of energetic particles in this region leads to enhanced fluxes of precipitating high energy ions and electrons that are higher than at other longitudes. This leads to enhanced collisions with the neutrals, and since the early days of space exploration it has been speculated that this can lead to the deposition of a significant amount of energy to the neutral atmosphere. Indications that the neutral temperatures could be higher in the SSA region than elsewhere have been provided early on, e.g. by Wulff and Gledhill (1974), Gledhill (1976) and references therein.

Instrumental/measurement effects are also known to be correlated to the SAA: for example, it is known that penetrating high energy particles can introduce enhanced noise in most instruments. This could be seen as enhanced background noise on the T_i signal as obtained from the RPA instrument, or the T_n signal from the NATE instrument, or in both signals.

From the results shown in Fig. 5 it is noted that, whereas the region of primary enhancement of the occurrence rates of $\Delta T_{in} < 0$, marked as A, reaches the vicinity of the SAA, however its peak is offset in terms of latitude and longitude to the North-East of the SAA; furthermore, it is noted that the SAA region is more restricted in latitude than the region of observations. Finally, plotting the same data shown Fig. 5 binned by altitude does not indicate a trend in altitude (results not shown herein). For example, SAA signatures would be expected to become more intense and restricted in longitude at low altitudes; hence an increase of the occurrence rates of $\Delta T_{in} < 0$ with decreasing altitude would signify a correlation with the SAA, which has not been identified herein. Further complicating the interpretation of these results, the appearance of the second largest peak in the occurrence rates of $\Delta T_{in} < 0$ in the vicinity of the Indian Ocean, marked as B in Fig. 5, can not be attributed to or be associated with the SAA.

Another mechanism that could significantly affect the dynamics and energetics of the thermosphere is related to the yet-unresolved phenomenon of the ionospheric plasma caves, the unusual decreases in electron density that are theoretically expected to occur in the equatorial regions. For example, Liu et al. (2010), Lee et al. (2012) and Chen et al. (2014) presented theoretical studies of the equatorial ionization anomaly region's ionospheric plasma cave based on FORMOSAT-3/COSMIC and Dynamic Explorer-2 (DE-2) and simulation, respectively. The plasma cave structures are attributed to neutral winds that are distinguished by two divergent wind zones at off-equator latitudes and a convergent wind region at the magnetic equator. Since electrons are mainly transferring energy to the ions, the absence of electrons within plasma caves are speculated to create

the conditions for the occurrences of neutrals that are hotter than ion. Plasma caves are expected through simulations to be observed between $\sim 0^o$–$\sim 120^o E$ longitudes, which is in rough agreement with the peaks marked as A and B in Fig. 5, over the south Atlantic region. They are also expected to show a significant latitudinal asymmetry, which is also observed in Fig. 5. However, as noted in Chen et al. (2014), there are considerable remaining discrepancies between simulations and observations of plasma caves, primarily due to unknowns in the distribution and structuring of neutral winds in the lower thermospheric altitudes.

Together with the above analyses that compares the temperatures of ions and neutrals in the ionosphere-thermosphere, the relative temperature of electrons and ions is of extreme importance to the state of the ionosphere. Whereas globally it is expected that it is much more common for T_e to be greater than T_i due to the effects of UV radiation, at times $T_i > T_e$ has also been observed, associated with storm-time enhanced Joule heating. For example, through analyzing EISCAT ISR data, Kofman and Lathuillere (1987) have shown profiles of very high ion temperatures (greater than 8000K), observed along geomagnetic field lines, which they attributed to frictional heating between fast moving species. Similarly, Buchert and Hoz (1988) also reported observations of very high ion temperatures (on the order of 12000K), which were not accompanied by commensurate changes in the electron temperature; they also attributed such cases of $T_i < T_e$ to Joule heating. Although believed to be less common, such events are expected to be energetically very significant. Such events are not analyzed statistically herein, and are the topic of a future study.

5   Summary and Conclusions

In this study, a comparison between in situ satellite (AE-C, AE-E and DE-2) and ISR (Arecibo, Millstone Hill and St. Santin) measurements of T_e and T_i has been performed. Through this comparison, it has been found that the agreement between satellite and ISR measurements is best for AE-C and AE-E, for both T_e and T_i, and is quantitatively similar to the results of Benson et al. (1977a) that focused on only AE-C measurements. The results presented herein show a larger discrepancy for DE-2, both in terms of the fits to the data and to the standard deviation, and indicate that DE-2 possibly over-estimates T_i, with deviations being higher for higher temperatures.

Through a re-analysis of ion and neutral temperatures, a surprisingly high occurrence rate of $\Delta T_{in} < 0$ is reported. Furthermore, an intriguing spatial distribution of the occurrences of $\Delta T_{in} < 0$ is presented, showing distinct peaks in the occurrence rates in (in order of significance): A. the South Atlantic Ocean; B. the Indian Ocean, C. the South-Western Pacific Ocean; D. the Eastern Pacific Ocean; E. North Mexico/Baja California; F. the Northern Atlantic Ocean; and G. the North-Eastern Pacific Ocean. A distinct lack of occurrences is observed at: H. all northern and southern high latitudes; I. over Europe and Northern Africa; J. Northern Russia.

Several potential causes have been identified that could explain the appearance of $\Delta T_{in} < 0$; these are summarised as follows:

- A ram cloud could produce ion temperatures that are cooler than the ambient neutrals; the deviation would be a function of neutral density. These could be observed at all latitudes and longitudes, at low altitudes. Detailed instrument-level simulations are needed to accurately subtract ram cloud effects from measurements.

- Gravity Waves (GW) can have significant thermal effects, leading to localized heating of the neutrals, but also to cooling. The parameterization of GWs and their distribution and occurrence, which are currently largely missing, will enable the exact quantification of their effects in terms of heating and cooling in the LTI.

- Precipitating particles in the South Atlantic Anomaly (SAA) can lead to an enhancement of neutral temperatures. The parameterization and localization of these effects requires detailed simulations.

- Plasma Caves, the regions where the unusual decrease of electron density is observed (Liu et al. (2010) and Chen et al. (2014)), can lead to a decrease of ion temperatures. Detailed simulations combined with in situ measurements of all relevant parameters could help resolve the regional and global effects of plasma caves.

- The equatorial region fountain effect, via the collisions between charged and neutral particles and the subsequent transfer of energy and momentum from the plasma to the neutral gas is also a candidate mechanisms. Detailed simulations combined with in situ measurements of all relevant parameters will help resolve the contributions of this effect on regional and global scales.

Whereas a single process can not be invoked to explain the spatial distribution of the occurrences of observations of $T_i < T_n$, it is possible that different causes can be at play in different regions and/or at different times. Whereas instrumental effects can not be excluded, the reported spatial distributions indicate that there are patterns in the occurrences of these events that hint to distinct underlying mechanisms that lead to either unexpectedly cool ion temperatures or unexpectedly warm neutral temperatures. It is noted that existing models cannot predict such observations of $T_i < T_n$, which highlights a lack of understanding of the underlying processes in the LTI. Recently, Peterson et al. (2023) also reported the appearance of cases where $\Delta T_{in} < 0$, and similarly concluded that there is so little that we know about the processes taking place in LTI region, and that, if $\Delta T_{in} < 0$ are real, they would emerge from unforeseen and unstudied physical processes; they also attributed such occurrences to high altitude gravity waves (England et al. (2020)).

The results presented herein are based on a re-analysis of the only available in-situ co-spatial and co-temporal datasets of T_i and T_n, from the early Atmosphere Explorer and Dynamics Explorer missions, with the exception of a few rocket flights. Even though non-conclusive, these results highlight the fact that the LTI region is one of the least explored regions of the Earth's atmosphere and that there is very limited knowledge about the ongoing processes. It also highlights the limitations of current observational techniques, such as ISRs, which can not simultaneously provide information about T_e, T_i and T_n. It is noted that observations of T_n in the lower thermosphere have also been provided via from space-born UV instruments, such as GUVI on the TIMED satellite (Christensen et al., 2003), which could be combined with remote sensing of T_e and T_i from ISR measurements; for example, recently, Peterson et al. (2023) presented examples of co-temporal, co-spatial observations of T_n from GUVI as well as T_e and T_i observations from incoherent scatter radars. In their conclusions, they point out that the error

bars on the presented temperature profile observations do not allow a strong conclusion to be drawn; however, a systematic statistical investigation of these combined datasets could yield more insight into the conditions leading to observations of $\Delta T_{in} < 0$.

In conclusion, it is noted that the combined and systematic measurement of all three T_e, T_i and T_n, ideally provided in-situ from instruments onboard the same platform, would allow us to conclusively assert on the thermal equilibrium between electrons, ions and neutrals, and to investigate the regions and causes of deviations from that state. Several studies have highlighted the need for comprehensive in situ measurements to address key unknowns in this region (e.g., Sarris (2019), Palmroth et al. (2021), Sarris et al. (2020), Sarris et al. (2023)); by providing significantly larger volumes of measurements than are currently available, such in situ missions will greatly enhance our understanding of the LTI region, including the underlying causes of the observations of $T_i < T_n$.

Data availability. ISR data are available through Madrigal Database http://cedar.openmadrigal.org/, accessed on 16 January 2022. AE-C, AE-D and AE-E satellite data are available though NASA's Space Physics Data Facility (SPDF: https://spdf.gsfc.nasa.gov/pub/data, accessed on 15 January 2020)

Appendix A: Supplementary Figures

Table A1. Orbit points and Temperature Measurements

	Total under 500km points	Total Te	Valid Te	Total Ti	Valid Ti	Total Tn	Valid Tn	Simultaneous Valid Te-Ti-Tn	Pos/Neg DTei	Pos/Neg DTin
AE-C	712517	569655	396895	441150	440893	83837	52876	48361	45892 / 2468	30689 / 17671
AE-D	95209	3755	3009	60670	60651	34473	11966	998	994 / 3	753 / 244
AE-E	517436	55198	34742	263984	263941	311953	171785	20180	20160 / 19	16837 / 3342
DE-2	411189	353860	255681	280686	277944	322872	237387	221702	161587 / 60114	212290 / 9411
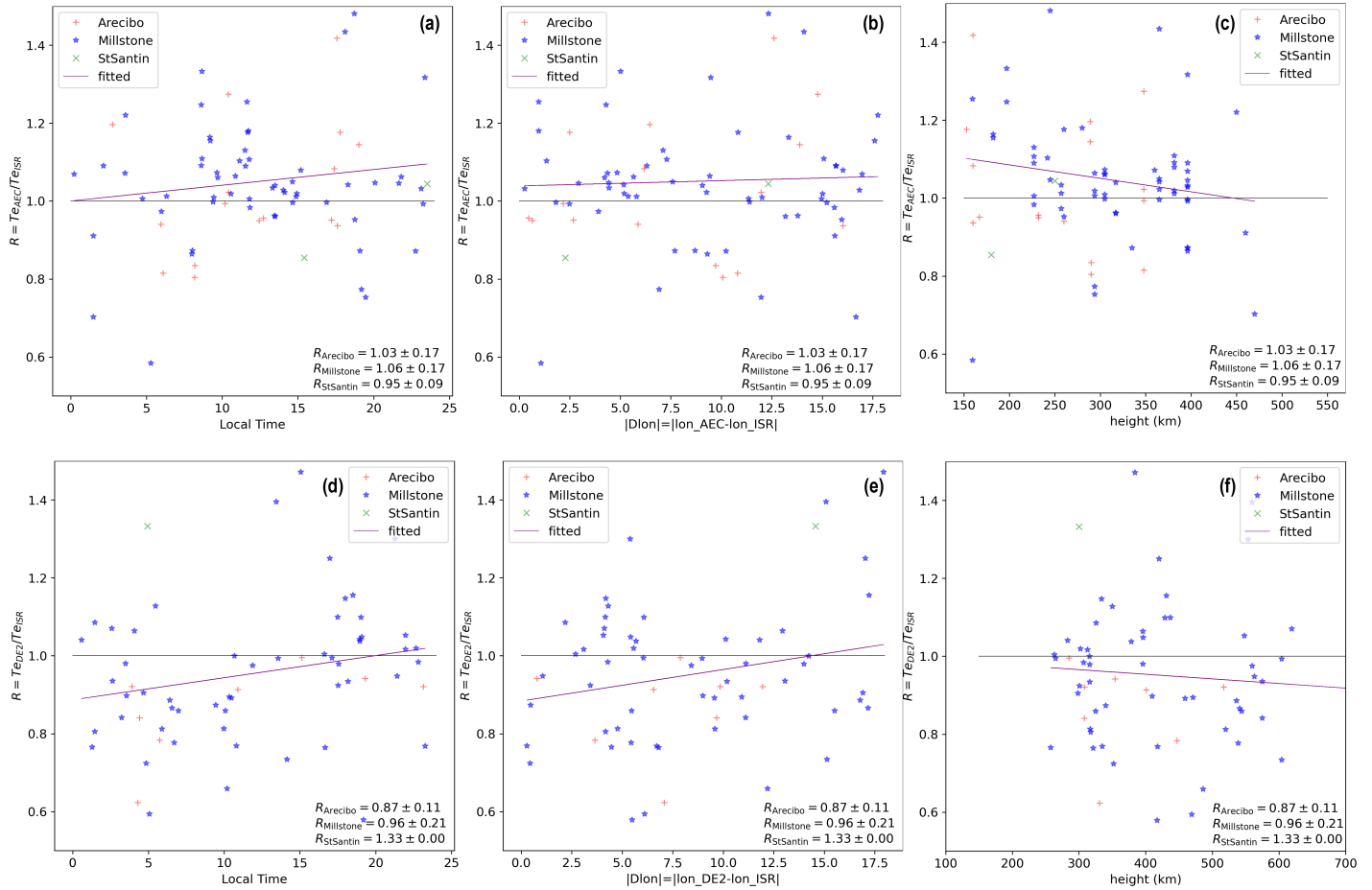
Figure A1. Te Ratio as a function of Local Time, Absolute Longitude Separation and Height for AE-C and DE-2 and ISRs. (a) AE-C Te Ratio as a function of Local Time, (b) AE-C Te Ratio as a function of Absolute Longitude Separation, (c) AE-C Te Ratio as a function of Height, (d) DE-2 Te Ratio as a function of Local Time, (e) DE-2 Te Ratio as a function of Absolute Longitude Separation, (f) DE-2 Te Ratio as a function of Height.
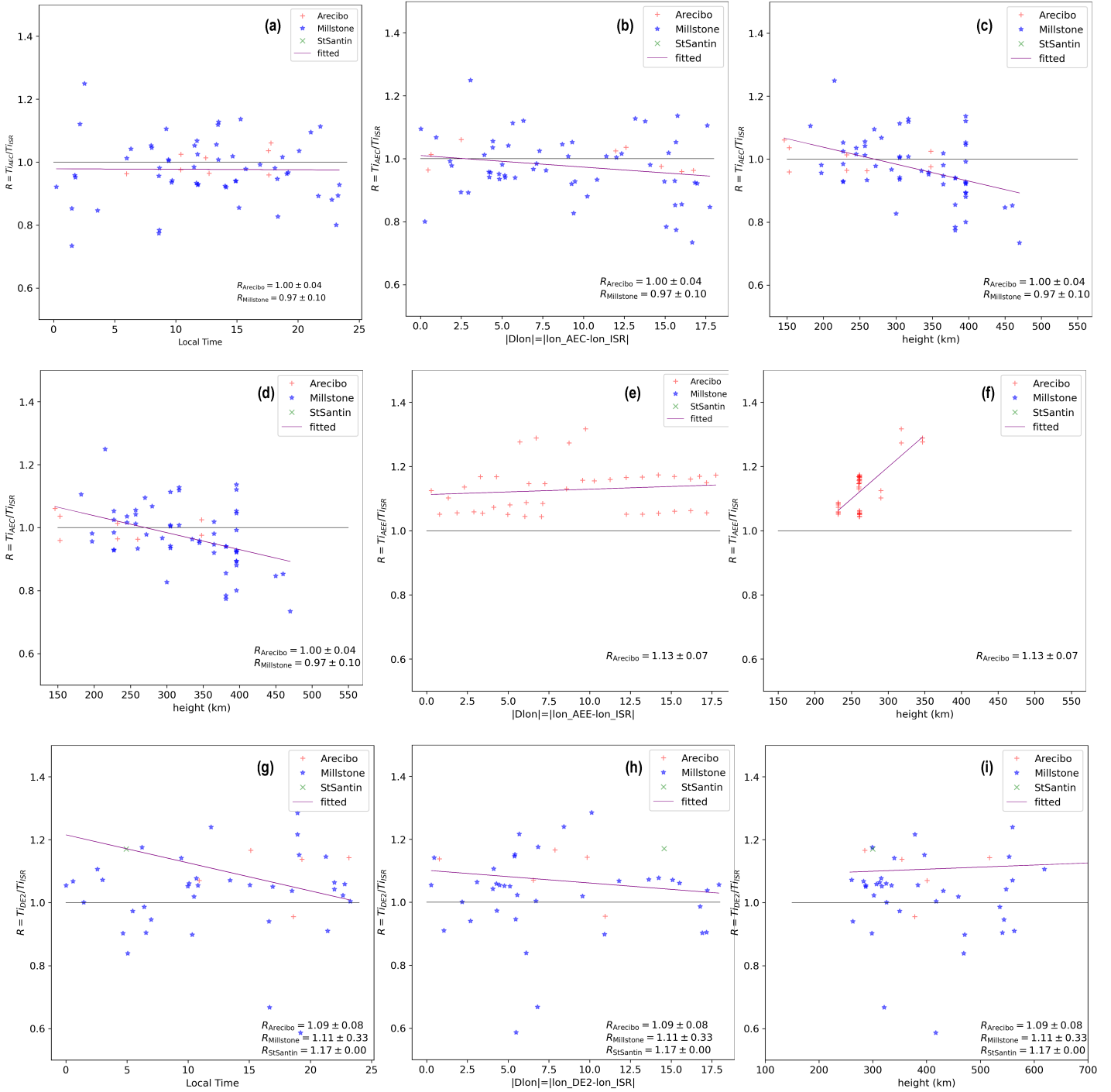
Figure A2. Ti Ratio as a function of Local Time, Absolute Longitude Separation and Height for AE-C and ISRs. (a) AE-C Ti Ratio as a function of Local Time, (b) AE-C Ti Ratio as a function of Absolute Longitude Separation, (c) AE-C Ti Ratio as a function of Height, (d) AE-E Ti Ratio as a function of Local Time, (e) AE-E Ti Ratio as a function of Absolute Longitude Separation, (f) AE-E Ti Ratio as a function of Height, (g) DE-2 Ti Ratio as a function of Local Time, (h) DE-2 Ti Ratio as a function of Absolute Longitude Separation, (i) DE-2 Ti Ratio as a function of Height.
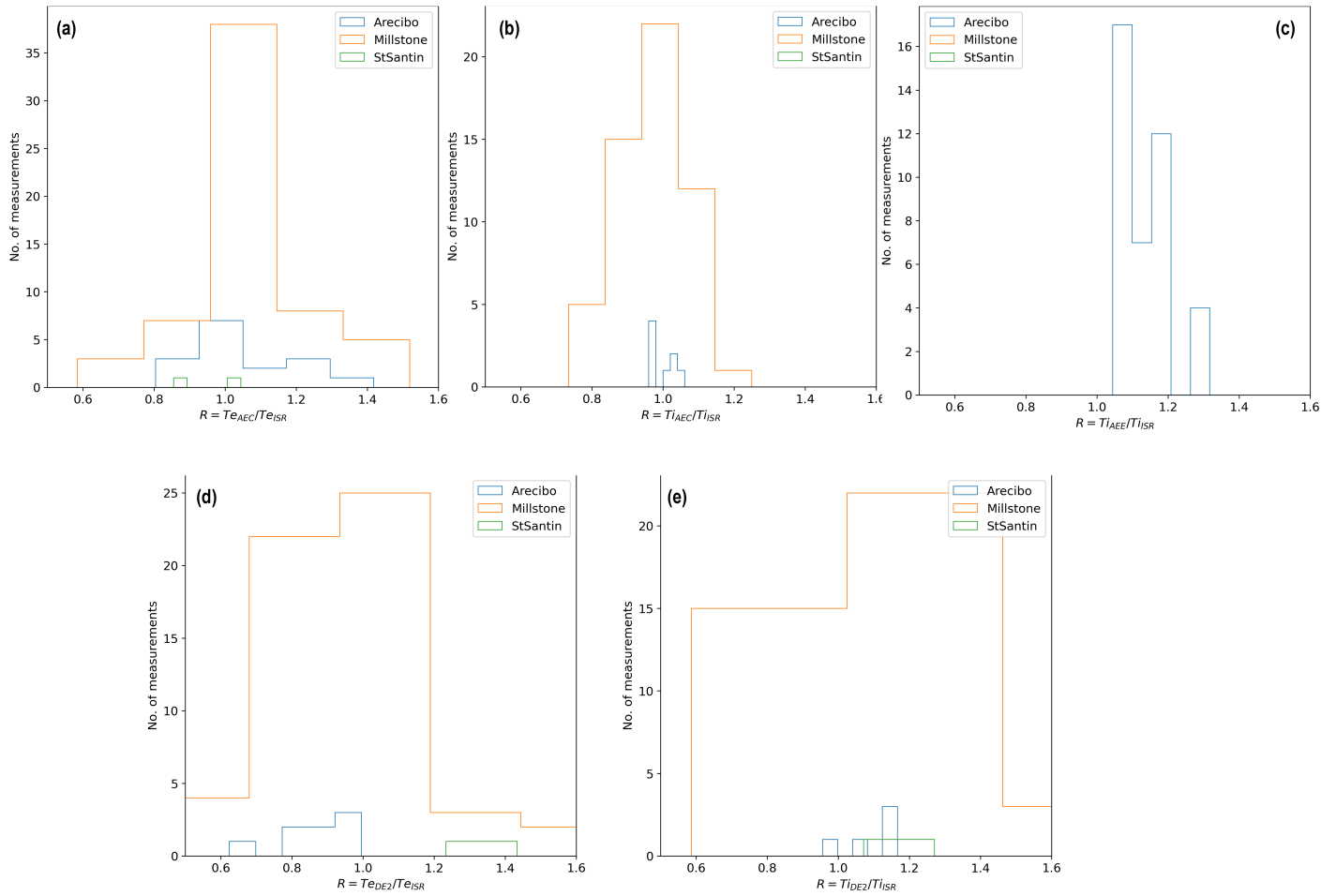
Figure A3. Distribution of Satellites vs. ISR Ratios. (a) AE-C Te Ratio, (b) AE-C Ti Ratio, (c) AE-E Ti Ratio, (d) DE-2 Te Ratio, (e) DE-2 Ti Ratio.
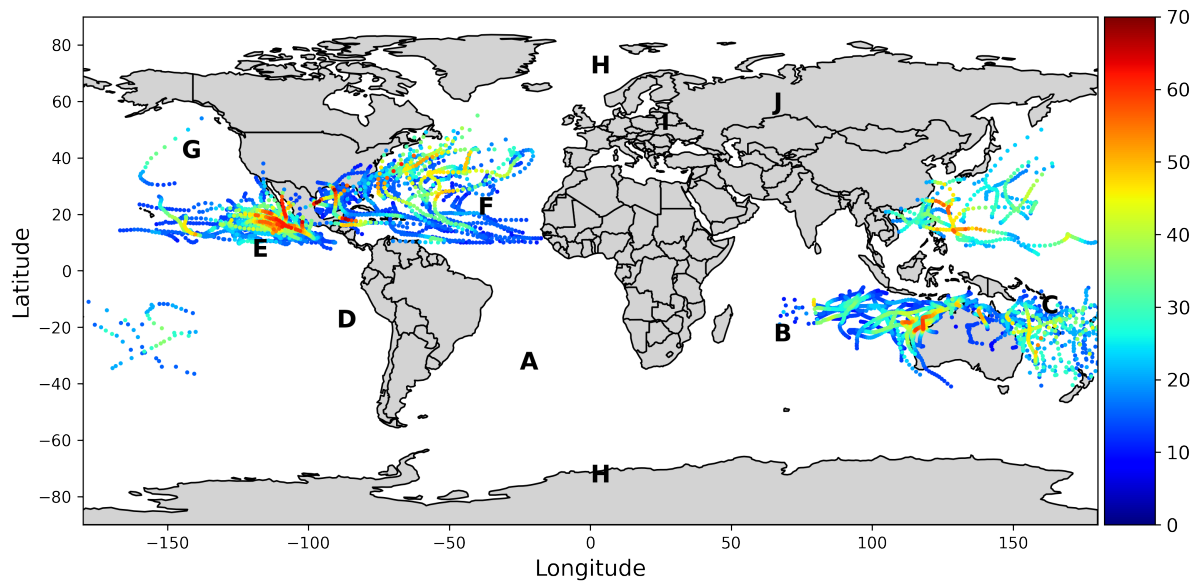
Figure A4. Typhoon and Tropical Cyclones between 1974 and 1978, color-scale in m/s

420 *Author contributions.* The authors confirm contribution to the paper as follows: study conception and design: PP, TS; data collection: PP; analysis and interpretation of results: PP, TS; PP prepared the manuscript with contribution from TS

Competing interests. The authors declare that they have no conflict of interest.

Acknowledgements. This research has been funded through DUTH grants KE82503, KE83030 and KE83048.

References

425 Andrews, D. G., Holton, J. R., and Leovy, C. B.: Middle atmosphere dynamics, https://www.osti.gov/biblio/5936274, 1987.

Becker, E., Goncharenko, L., Harvey, V. L., and Vadas, S. L.: Multi-Step Vertical Coupling During the January 2017 Sudden Stratospheric Warming, Journal of Geophysical Research: Space Physics, 127, e2022JA030 866, https://doi.org/https://doi.org/10.1029/2022JA030866, e2022JA030866 2022JA030866, 2022.

Benson, R. F., Bauer, P., Brace, L. H., Carlson, H. C., Hagen, J., Hanson, W. B., Hoegy, W. R., Torr, M. R., Wand, R. H., and Wickwar, V. B.:
430 Electron and ion temperatures-A comparison of ground-based incoherent scatter and AE-C satellite measurements, Journal of Geophysical Research, 82, 36–42, https://doi.org/10.1029/ja082i001p00036, 1977a.

Benson, R. F., Bauer, P., Brace, L. H., Carlson, H. C., Hagen, J., Hanson, W. B., Hoegy, W. R., Torr, M. R., Want, R. H., and Wickwar, Y. B.:
Electron and ion temperatures - A comparison of ground-based incoherent scatter and AE-C satellite measurements, J. Geophys. Res. 82, 82, 36–42, 1977b.

435 Bilitza, D., Rawer, K., Bossy, L., and Gulyaeva, T.: International reference ionosphere — past, present, and future: II. Plasma temperatures, ion composition and ion drift, Advances in Space Research, 13, 15–23, https://doi.org/https://doi.org/10.1016/0273-1177(93)90241-3, 1993.

Bilitza, D., Pezzopane, M., Truhlik, V., Altadill, D., Reinisch, B. W., and Pignalberi, A.: The International Reference Ionosphere Model: A Review and Description of an Ionospheric Benchmark, Reviews of Geophysics, 60, e2022RG000 792,
440 https://doi.org/https://doi.org/10.1029/2022RG000792, e2022RG000792 2022RG000792, 2022.

Billingsley, P.: Probability and Measure, John Wiley and Sons, second edn., 1986.

Block, L. P.: A double layer review, Astrophysics and Space Science, 55, 59–83, https://doi.org/10.1007/bf00642580, 1978.

Brace, L. H., Theis, R. F., and Dalgarno, A.: The cylindrical electrostatic probes for Atmosphere Explorer C, D and E, Radio Science, 8, 341–348, 1973.

445 Buchert, S. and Hoz, C. L.: Extreme ionospheric effects in the presence of high electric fields, Nature, 333, 438–440, 1988.

Burch, J. and Hoffman, R.: Introduction to the Dynamics Explorer mission, in: 23rd Aerospace Sciences Meeting, American Institute of Aeronautics and Astronautics, https://doi.org/10.2514/6.1985-61, 1985.

Carignan, G. R., Block, B. P., Maurer, J. C., Hedin, A. E., Reber, C. A., and Spencer, N. W.: The neutral mass spectrometer on Dynamics Explorer B, Space Science Instrumentation, 5, 429–441, http://inis.iaea.org/search/search.aspx?orig_q=RN:13668476, 1981.

450 Chandra, S., Spencer, N. W., Krankowsky, D., and Lammerzahl, P.: A Comparison of Measured and Inferred Temperatures from Aeros-B, Geophys. Res. Ltrs., 3, 1976.

Chen, S.-L. and Sekiguchi, T.: Instantaneous Direct-Display System of Plasma Parameters by Means of Triple Probe, Journal of Applied Physics, 36, 2363–2375, https://doi.org/10.1063/1.1714492, 1965.

Chen, Y.-T., Lin, C. H., Chen, C. H., Liu, J. Y., Huba, J. D., Chang, L. C., Liu, H.-L., Lin, J. T., and Rajesh, P. K.: Theoretical study of
455 the ionospheric plasma cave in the equatorial ionization anomaly region, Journal of Geophysical Research: Space Physics, 119, 10,324–10,335, https://doi.org/https://doi.org/10.1002/2014JA020235, 2014.

Christensen, A. B., Paxton, L. J., Avery, S., Craven, J., Crowley, G., Humm, D. C., Kil, H., Meier, R. R., Meng, C.-I., Morrison, D., Ogorzalek, B. S., Straus, P., Strickland, D. J., Swenson, R. M., Walterscheid, R. L., Wolven, B., and Zhang, Y.: Initial observations with the Global Ultraviolet Imager (GUVI) in the NASA TIMED satellite mission, Journal of Geophysical Research: Space Physics, 108,
460 https://doi.org/https://doi.org/10.1029/2003JA009918, 2003.

Dalgarno, A., Hanson, W. B., Spencer, N. W., and Schmerling, E. R.: The Atmosphere Explorer mission, Radio Science, 8, 263–266, https://doi.org/https://doi.org/10.1029/RS008i004p00263, 1973.

DeForest, S. E.: Spacecraft charging at synchronous orbit, Journal of Geophysical Research (1896-1977), 77, 651–659, https://doi.org/https://doi.org/10.1029/JA077i004p00651, 1972.

465 Dobbin, A. L.: Modelling studies of possible coupling mechanisms between the upper and middle atmosphere, University of London, University College London (United Kingdom), 2005.

Emmert, J. T., Drob, D. P., Picone, J. M., Siskind, D. E., Jones Jr., M., Mlynczak, M. G., Bernath, P. F., Chu, X., Doornbos, E., Funke, B., Goncharenko, L. P., Hervig, M. E., Schwartz, M. J., Sheese, P. E., Vargas, F., Williams, B. P., and Yuan, T.: NRLMSIS 2.0: A Whole-Atmosphere Empirical Model of Temperature and Neutral Species Densities, Earth and Space Science, 8, e2020EA001 321,

470 https://doi.org/https://doi.org/10.1029/2020EA001321, e2020EA001321 2020EA001321, 2021.

England, S. L., Greer, K. R., Solomon, S. C., Eastes, R. W., McClintock, W. E., and Burns, A. G.: Observation of Thermospheric Gravity Waves in the Southern Hemisphere With GOLD, Journal of Geophysical Research: Space Physics, 125, e2019JA027 405, https://doi.org/https://doi.org/10.1029/2019JA027405, e2019JA027405 2019JA027405, 2020.

Ergun, R. E., Andersson, L. A., Fowler, C. M., and Thaller, S. A.: Kinetic Modeling of Langmuir Probes in Space and Applica-

475 tion to the MAVEN Langmuir Probe and Waves Instrument, Journal of Geophysical Research: Space Physics, 126, e2020JA028 956, https://doi.org/https://doi.org/10.1029/2020JA028956, e2020JA028956 2020JA028956, 2021.

Fritts, D. C. and Alexander, M. J.: Gravity wave dynamics and effects in the middle atmosphere, Reviews of Geophysics, 41, https://doi.org/https://doi.org/10.1029/2001RG000106, 2003.

Ginzburg, V., Kurnosova, L., Logachev, V., Rozarenov, L., Sirotkin, I., and Fradkin, M.: Investigation of charged particle intensity during

480 the flights of the second and third space-ships, Planetary and Space Science, 9, 845–846, https://doi.org/https://doi.org/10.1016/0032-0633(62)90113-7, 1962.

Gledhill, J. A.: Aeronomic effects of the South Atlantic Anomaly, Reviews of Geophysics, 14, 173–187, https://doi.org/https://doi.org/10.1029/RG014i002p00173, 1976.

Hanley, K. G., McFadden, J. P., Mitchell, D. L., Fowler, C. M., Stone, S. W., Yelle, R. V., Mayyasi, M., Ergun, R. E., Andersson, L.,

485 Benna, M., Elrod, M. K., and Jakosky, B. M.: In Situ Measurements of Thermal Ion Temperature in the Martian Ionosphere, Journal of Geophysical Research: Space Physics, 126, e2021JA029 531, https://doi.org/https://doi.org/10.1029/2021JA029531, e2021JA029531 2021JA029531, 2021.

Hanson, W. B. and Heelis, R. A.: Techniques for measuring bulk gas-motions from satellites, Spa. Sci. Instrum., 1, 1975.

Hanson, W. B., Frame, D. R., and Midgley, J. E.: Errors in retarding potential analyzers caused by nonuniformity of the grid-plane potential,

490 Journal of Geophysical Research, 77, 1914–1922, https://doi.org/10.1029/ja077i010p01914, 1972.

Hanson, W. B., Zuccaro, D. R., Lippincott, C. R., and Sanatani, S.: The retarding potential analyzer on Atmosphere Explorer, Radio Sci., 8, 333, 1973.

Hanson, W. B., Heelis, R. A., Power, R. A., Lippincott, C. R., Zuccaro, D. R., Holt, B. J., Harmon, L. H., and Sanatani, S.: The Retarding Potential Analyzer for Dynamics Explorer-B, Space Science Instrumentation, 5, 503–510, 1981.

495 Harris, M. J.: A new coupled middle atmosphere and thermosphere general circulation model: Studies of dynamic, energetic and photochemical coupling in the middle and upper atmosphere, University of London, University College London (United Kingdom), 2001.

Hastings, D. E.: A review of plasma interactions with spacecraft in low Earth orbit, Journal of Geophysical Research: Space Physics, 100, 14 457–14 483, https://doi.org/https://doi.org/10.1029/94JA03358, 1995.

Heelis, R. A. and Hanson, W. B.: Measurement Techniques in Space Plasmas, no. 102 in Geophysical Monograph Series, American Geo-
physical Union (AGU), Washington, D.C., 1998.

Hierro, R., Steiner, A. K., de la Torre, A., Alexander, P., Llamedo, P., and Cremades, P.: Orographic and convective gravity waves above the
Alps and Andes Mountains during GPS radio occultation events – a case study, Atmospheric Measurement Techniques, 11, 3523–3539,
https://doi.org/10.5194/amt-11-3523-2018, 2018.

Hopwood, J., Guarnieri, C. R., Whitehair, S. J., and Cuomo, J. J.: Langmuir probe measurements of a radio frequency induction plasma,
Journal of Vacuum Science & Technology A: Vacuum, Surfaces, and Films, 11, 152–156, https://doi.org/10.1116/1.578282, 1993.

Jakosky, B. M., Lin, R. P., Grebowsky, J. M., Luhmann, J. G., Mitchell, D., Beutelschies, G., Priser, T., Acuna, M., Andersson, L., Baird, D.,
et al.: The Mars atmosphere and volatile evolution (MAVEN) mission, Space Science Reviews, 195, 3–48, 2015.

Knapp, K. R., Kruk, M. C., Levinson, D. H., Diamond, H. J., and Neumann, C. J.: The International Best Track Archive for Cli-
mate Stewardship (IBTrACS): Unifying Tropical Cyclone Data, Bulletin of the American Meteorological Society, 91, 363 – 376,
https://doi.org/https://doi.org/10.1175/2009BAMS2755.1, 2010.

Knapp, K. R., Diamond, H. J., Kossin, J. P., Kruk, M. C., and Schreck, C. J.: International Best Track Archive for Climate Stewardship
(IBTrACS) Project, Version 4, https://doi.org/10.25921/82TY-9E16, 2018.

Kofman, W. and Lathuillere, C.: Observation by the incoherent scatter technique of the hot spots in the auroral zone ionosphere, Geophysical
research letters, 14, 1158–1161, 1987.

Lee, I. T., Liu, J. Y., Lin, C. H., Oyama, K.-I., Chen, C. Y., and Chen, C. H.: Ionospheric plasma caves under the equatorial ionization
anomaly, Journal of Geophysical Research: Space Physics, 117, https://doi.org/https://doi.org/10.1029/2012JA017868, 2012.

Liu, H.-L.: Quantifying gravity wave forcing using scale invariance, Nature Communications, 10, https://doi.org/10.1038/s41467-019-10527-
z, 2019.

Liu, J. Y., Lin, C. Y., Lin, C. H., Tsai, H. F., Solomon, S. C., Sun, Y. Y., Lee, I. T., Schreiner, W. S., and Kuo, Y. H.: Artificial plasma cave in
the low-latitude ionosphere results from the radio occultation inversion of the FORMOSAT-3/COSMIC, Journal of Geophysical Research:
Space Physics, 115, https://doi.org/https://doi.org/10.1029/2009JA015079, 2010.

NASA, W.: WATS Description Processing, https://spdf.gsfc.nasa.gov/pub/data/de/de/neutral_gas_wats/description_processing.txt, 1998.

Nenovski, P., Kutiev, I., and Karadimov, M.: Effect of RPA transparency dependence on ion masses upon ion temperature and density
determination with direct space measurements, Journal of Physics E: Scientific Instruments, 13, 1011–1016, https://doi.org/10.1088/0022-
3735/13/9/028, 1980.

Palmroth, M., Grandin, M., Sarris, T., Doornbos, E., Tourgaidis, S., Aikio, A., Buchert, S., Clilverd, M. A., Dandouras, I., Heelis, R.,
Hoffmann, A., Ivchenko, N., Kervalishvili, G., Knudsen, D. J., Kotova, A., Liu, H.-L., Malaspina, D. M., March, G., Marchaudon, A.,
Marghitu, O., Matsuo, T., Miloch, W. J., Moretto-Jørgensen, T., Mpaloukidis, D., Olsen, N., Papadakis, K., Pfaff, R., Pirnaris, P., Siemes,
C., Stolle, C., Suni, J., van den IJssel, J., Verronen, P. T., Visser, P., and Yamauchi, M.: Lower-thermosphere–ionosphere (LTI) quantities:
current status of measuring techniques and models, Annales Geophysicae, 39, 189–237, https://doi.org/10.5194/angeo-39-189-2021, 2021.

Peterson, W. K.: Perspective on Energetic and Thermal Atmospheric Photoelectrons, Frontiers in Astronomy and Space Sciences, 8,
https://doi.org/10.3389/fspas.2021.655309, 2021.

Peterson, W. K., Maruyama, N., Richards, P., Erickson, P. J., Christensen, A. B., and Yau, A. W.: What Is the Altitude of Thermal Equi-
librium?, Geophysical Research Letters, 50, e2023GL102 758, https://doi.org/https://doi.org/10.1029/2023GL102758, e2023GL102758
2023GL102758, 2023.

Pfaff, R. F.: The Near-Earth Plasma Environment, Space Science Reviews, 168, 23–112, https://doi.org/10.1007/s11214-012-9872-6, 2012.

Picone, J. M., Hedin, A. E., Drob, D. P., and Aikin, A. C.: NRLMSISE-00 empirical model of the atmosphere: Statistical comparisons and scientific issues, Journal of Geophysical Research: Space Physics, 107, SIA 15–1–SIA 15–16, https://doi.org/https://doi.org/10.1029/2002JA009430, 2002.

540 Pirnaris, P. and Sarris, T. E.: Common Observations/measurements Between Incoherent Scatter Radars (ISR) and Atmosphere Explorers (AE) -C, -D, -E, Dynamic Explorer 2, https://doi.org/10.5281/zenodo.7967432, 2023.

Richards, P. G.: Ionospheric photoelectrons: A lateral thinking approach, Frontiers in Astronomy and Space Sciences, 9, https://doi.org/10.3389/fspas.2022.952226, 2022.

Rosenblatt, M.: Remarks on Some Nonparametric Estimates of a Density Function, The Annals of Mathematical Statistics, 27, 832 – 837,
545 https://doi.org/10.1214/aoms/1177728190, 1956.

Rossini, A. J.: "Applied Smoothing Techniques for Data Analysis: The Kernel Approach with S-Plus Illustrations" by Adrian W. Bowman and Adelchi Azzalini, Computational Statistics, 15, 301–302, https://doi.org/10.1007/s001800000033, 2000.

Sarris, T., Palmroth, M., Aikio, A., Buchert, S. C., Clemmons, J., Clilverd, M., Dandouras, I., Doornbos, E., Goodwin, L. V., Grandin, M., Heelis, R., Ivchenko, N., Moretto-Jørgensen, T., Kervalishvili, G., Knudsen, D., Liu, H.-L., Lu, G., Malaspina, D. M., Marghitu, O.,
550 Maute, A., Miloch, W. J., Olsen, N., Pfaff, R., Stolle, C., Talaat, E., Thayer, J., Tourgaidis, S., Verronen, P. T., and Yamauchi, M.: Plasma-neutral interactions in the lower thermosphere-ionosphere: The need for in situ measurements to address focused questions, Frontiers in Astronomy and Space Sciences, 9, https://doi.org/10.3389/fspas.2022.1063190, 2023.

Sarris, T. E.: Understanding the ionosphere thermosphere response to solar and magnetospheric drivers: status, challenges and open issues, Philosophical Transactions of the Royal Society A: Mathematical, Physical and Engineering Sciences, 377, 20180 101,
555 https://doi.org/10.1098/rsta.2018.0101, 2019.

Sarris, T. E., Talaat, E. R., Palmroth, M., Dandouras, I., Armandillo, E., Kervalishvili, G., Buchert, S., Tourgaidis, S., Malaspina, D. M., Jaynes, A. N., Paschalidis, N., Sample, J., Halekas, J., Doornbos, E., Lappas, V., Moretto Jørgensen, T., Stolle, C., Clilverd, M., Wu, Q., Sandberg, I., Pirnaris, P., and Aikio, A.: Daedalus: a low-flying spacecraft for in situ exploration of the lower thermosphere–ionosphere, Geoscientific Instrumentation, Methods and Data Systems, 9, 153–191, https://doi.org/10.5194/gi-9-153-2020, 2020.

560 Sasaki, S. and Kawashima, N.: rocket measurement of ion and neutral temperatures in the lower ionosphere, Journal of Geophysical Research (1896-1977), 80, 2824–2828, https://doi.org/https://doi.org/10.1029/JA080i019p02824, 1975a.

Sasaki, S. and Kawashima, N.: rocket measurement of ion and neutral temperatures in the lower ionosphere, Journal of Geophysical Research, 80, 2824–2828, 1975b.

Schunk, R. and Nagy, A.: Ionospheres: Physics, Plasma Physics, and Chemistry, Cambridge Atmospheric and Space Science Series, Cam-
565 bridge University Press, 2 edn., https://doi.org/10.1017/CBO9780511635342, 2009.

Schwabedissen, A., Benck, E. C., and Roberts, J. R.: Langmuir probe measurements in an inductively coupled plasma source, Physical Review E, 55, 3450–3459, https://doi.org/10.1103/physreve.55.3450, 1997.

Scott, D. W.: Multivariate Density Estimation, Wiley, https://doi.org/10.1002/9780470316849, 1992.

Spencer, N. W., H, U. N., and Carignan, G. R.: The Neutral-Atmosphere Temperature Instrument, Radio Science, 8, 1973a.

570 Spencer, N. W., Niemann, H. B., and Carignan, G. R.: The neutral-atmosphere temperature instrument, Radio Science, 8, 287–296, https://doi.org/https://doi.org/10.1029/RS008i004p00287, 1973b.

Spencer, N. W., Pelz, D. T., Niemann, H. B., Carignan, G. R., and Caldwell, J. R.: The Neutral Atmosphere Temperature Experiment, J. Geophys., 40, 1974.

Spencer, N. W., Theis, R. F., Wharton, L. E., and Carignan, G. R.: Local Vertical Motions and Kinetic Temperature from AE-C as Evidence for Aurora-Induced Gravity Waves, Geophys. Res. Ltrs., 3, 1976.

Stanojević, M., Čerček, M., and Gyergyek, T.: Experimental Study of Planar Langmuir Probe Characteristics in Electron Current-Carrying Magnetized Plasma, Contributions to Plasma Physics, 39, 197–222, https://doi.org/10.1002/ctpp.2150390303, 1999.

Vadas, S. L. and Azeem, I.: Concentric Secondary Gravity Waves in the Thermosphere and Ionosphere Over the Continental United States on March 25–26, 2015 From Deep Convection, Journal of Geophysical Research: Space Physics, 126, e2020JA028 275, https://doi.org/https://doi.org/10.1029/2020JA028275, e2020JA028275 2020JA028275, 2021.

Vernov, S. and Chudakov, A.: Terrestrial corpuscular radiation and cosmic rays, Space Research, p. 751, 1960.

Walterscheid, R. L.: Dynamical cooling induced by dissipating internal gravity waves, Geophysical Research Letters, 8, 1235–1238, https://doi.org/https://doi.org/10.1029/GL008i012p01235, 1981.

Whipple, E. C.: Potentials of surfaces in space, Reports on Progress in Physics, 44, 1197, https://doi.org/10.1088/0034-4885/44/11/002, 1981.

Whipple, Jr, E. C.: THE ION-TRAP RESULTS IN "EXPLORATION OF THE UPPER ATMOSPHERE WITH THE HELP OF THE THIRD SOVIET SPUTNIK", https://www.osti.gov/biblio/4108305, 1961.

Wulff, A. and Gledhill, J.: Atmospheric ionization by precipitated electrons, Journal of Atmospheric and Terrestrial Physics, 36, 79–91, https://doi.org/https://doi.org/10.1016/0021-9169(74)90068-3, 1974.

Yiğit, E. and Medvedev, A. S.: Heating and cooling of the thermosphere by internal gravity waves, Geophysical Research Letters, 36, https://doi.org/https://doi.org/10.1029/2009GL038507, 2009.

Yoshida, S., Ludwig, G. H., and Van Allen, J. A.: Distribution of trapped radiation in the geomagnetic field, Journal of Geophysical Research (1896-1977), 65, 807–813, https://doi.org/https://doi.org/10.1029/JZ065i003p00807, 1960.